

## Dynamics of Protein and Peptide Hydration

Kristofer Modig,<sup>†</sup> Edvards Liepinsh,<sup>‡</sup> Gottfried Otting,<sup>‡,§</sup> and Bertil Halle<sup>\*,†</sup>

*Contribution from the Department of Biophysical Chemistry, Lund University, SE-22100 Lund, Sweden, and Department of Medical Biochemistry and Biophysics, Karolinska Institute, SE-17177 Stockholm, Sweden*

Received September 4, 2003; E-mail: bertil.halle@bpc.lu.se

**Abstract:** Biological processes often involve the surfaces of proteins, where the structural and dynamic properties of the aqueous solvent are modified. Information about the dynamics of protein hydration can be obtained by measuring the magnetic relaxation dispersion (MRD) of the water <sup>2</sup>H and <sup>17</sup>O nuclei or by recording the nuclear Overhauser effect (NOE) between water and protein protons. Here, we use the MRD method to study the hydration of the cyclic peptide oxytocin and the globular protein BPTI in deeply supercooled solutions. The results provide a detailed characterization of water dynamics in the hydration layer at the surface of these biomolecules. More than 95% of the water molecules in contact with the biomolecular surface are found to be no more than two-fold motionally retarded as compared to bulk water. In contrast to small nonpolar molecules, the retardation factor for BPTI showed little or no temperature dependence, suggesting that the exposed nonpolar residues do not induce clathrate-like hydrophobic hydration structures. New NOE data for oxytocin and published NOE data for BPTI were analyzed, and a mutually consistent interpretation of MRD and NOE results was achieved with the aid of a new theory of intermolecular dipolar relaxation that accounts explicitly for the dynamic perturbation at the biomolecular surface. The analysis indicates that water–protein NOEs are dominated by long-range dipolar couplings to bulk water, unless the monitored protein proton is near a partly or fully buried hydration site where the water molecule has a long residence time.

### 1. Introduction

Most proteins and other biomolecules have been adapted by evolution to function optimally in aqueous environments. Protein–water interactions therefore play an essential role in the folding, stability, dynamics, and function of proteins. Conceptually, the problem may be analyzed in terms of different perturbation orders. The first-order effect of the bulk solvent on the protein is often described by solvent-averaged potentials, as in the dielectric screening of Coulomb interactions. To second order, we must acknowledge that the protein modifies the properties of the adjacent solvent and that this modification reacts back on the protein. The term hydration usually refers to such second-order effects, which range from the highly specific entrapment of structural water molecules in internal cavities to the generic perturbation of the water layer covering the external protein surface. In the present work, we examine to what extent the dynamics of the hydration layer differs from that of bulk water. This is an important question because the primary events in most biological processes, such as enzymatic catalysis, association, and recognition, take place at the protein–water interface. Moreover, because the volume of the hydration monolayer is comparable to the dry volume of a small protein, even a small perturbation of the hydration layer can have a large effect on protein energetics and dynamics.

Much of the experimental information about protein hydration dynamics has come from magnetic relaxation experiments using two different NMR techniques: magnetic relaxation dispersion (MRD) of the quadrupolar <sup>2</sup>H and <sup>17</sup>O nuclei in the water molecule<sup>1,2</sup> and intermolecular <sup>1</sup>H–<sup>1</sup>H nuclear Overhauser effects (NOEs) between water and protein protons.<sup>3,4</sup> Neither method can separately observe the hydration layer, because fast water exchange between hydration sites and bulk solvent makes the water (<sup>1</sup>H, <sup>2</sup>H, or <sup>17</sup>O) resonance degenerate. Nevertheless, different classes of water molecules can be identified and characterized. In the MRD method, a dynamic selection is accomplished by exploiting the fact that water molecules with different rotational correlation times give rise to characteristic frequency dependencies (dispersions) in the longitudinal relaxation rate  $R_1$ .<sup>1,2</sup> In the NOE method, the selection is more complicated, being dependent on both the dynamics and the spatial proximity of water molecules to protein protons with resolved <sup>1</sup>H resonances.<sup>3,4</sup> While the MRD<sup>5–7</sup> and NOE<sup>8–10</sup> methods are well-established and complementary tools for

- (1) Halle, B.; Denisov, V. P.; Venu, K. In *Biological Magnetic Resonance*; Krishna, N. R., Berliner, L. J., Eds.; Kluwer/Plenum: New York, 1999; pp 419–484.
- (2) Halle, B.; Denisov, V. P. *Methods Enzymol.* **2001**, *338*, 178–201.
- (3) Otting, G.; Liepinsh, E. *Acc. Chem. Res.* **1995**, *28*, 171–177.
- (4) Otting, G. *Prog. Nucl. Magn. Reson. Spectrosc.* **1997**, *31*, 259–285.
- (5) Denisov, V. P.; Peters, J.; Hörlein, H. D.; Halle, B. *Nat. Struct. Biol.* **1996**, *3*, 505–509.
- (6) Denisov, V. P.; Halle, B. *Faraday Discuss.* **1996**, *103*, 227–244.
- (7) Halle, B. In *Hydration Processes in Biology*; Bellissent-Funel, M.-C., Ed.; IOS Press: Dordrecht, 1998; pp 233–249.
- (8) Otting, G.; Wüthrich, K. *J. Am. Chem. Soc.* **1989**, *111*, 1871–1875.

<sup>†</sup> Lund University.

<sup>‡</sup> Karolinska Institute.

<sup>§</sup> Present address: Australian National University, Research School of Chemistry, Canberra, ACT 0200, Australia.

identifying and characterizing internal water molecules buried inside proteins, their application to the study of surface hydration presents experimental challenges as well as theoretical problems.

The problem faced in MRD studies of surface hydration is that virtually all water molecules interacting with a protein surface have rotational correlation times shorter than 1 ns at normal temperatures, so that the corresponding dispersions occur above the highest experimentally accessible ( $^2\text{H}$  or  $^{17}\text{O}$ ) frequency of about 100 MHz. MRD experiments can then yield only the average rotational correlation time for the inhomogeneous hydration layer. If the correlation time distribution has a weak long-time tail, as suggested by physical considerations, the average will be heavily influenced by a small number of strongly motionally retarded water molecules, presumably located in deep surface pockets.<sup>6,7</sup> Here, we report new MRD experiments that allow a more detailed characterization of surface hydration dynamics. This is accomplished by using an emulsion technique to study supercooled protein and peptide solutions down to  $-30\text{ }^\circ\text{C}$ . Because of the order-of-magnitude retardation of molecular motions at such temperatures, some of the water molecules at the protein surface give rise to observable dispersions, thereby allowing us to determine their correlation times and, by implication, their residence times. By varying the temperature, we can thus partly deconvolute the correlation time distribution.

In previous NOE studies of surface hydration,<sup>3,4,11–14</sup> it was assumed that observed NOEs are dominated by one or a few water molecules residing near a given protein proton. However, unless such nearby water molecules are motionally retarded by several orders of magnitude (as for internal water molecules), the observed NOE contains significant contributions from thousands of water molecules; that is, it is long-ranged.<sup>15</sup> To obtain information about the translational dynamics of hydration water, it is then necessary to use a model that allows the water self-diffusion coefficient in the hydration layer to differ from that in the bulk solvent. Such a nonuniform diffusion model has recently been developed,<sup>15</sup> and we use it here to interpret experimental NOE data.

The aim of the present work is two-fold: to characterize protein and peptide surface hydration dynamics in greater detail than hitherto possible and to examine whether the MRD and NOE methods yield mutually consistent results. To this end, we report low-temperature  $^2\text{H}$  and  $^{17}\text{O}$  MRD data for the cyclic nonapeptide oxytocin and the 6.5 kDa globular protein bovine pancreatic trypsin inhibitor (BPTI). These results are compared to NOE data for oxytocin at  $-25\text{ }^\circ\text{C}$ , acquired with improved methodology, and with previously published NOE data for BPTI at  $4\text{ }^\circ\text{C}$ .<sup>11,16,17</sup> Because the emulsion adversely affects spectral resolution, the NOE measurements on oxytocin used a water/

acetone cryosolvent,<sup>18</sup> which was also investigated by MRD. Previously, MRD and NOE results have been compared quantitatively only for DNA hydration.<sup>19,20</sup>

## 2. Materials and Methods

**2.1. Peptide and Protein Samples.** The trifluoroacetate salt of oxytocin was obtained from Bachem Feinchemikalien AG (Bubendorf, Switzerland). According to the manufacturer's HPLC analysis (lot no. 508590), the purity was 99.1%. Aqueous solutions of oxytocin were prepared by weight using water containing 50%  $^2\text{H}$  and 17%  $^{17}\text{O}$  (MRD samples) or 10%  $^2\text{H}$  (NOE sample). pH\* (uncorrected for isotope effects) was adjusted by microliter additions of HCl and NaOH. The emulsion sample was made by mixing equal volumes of 41 mM aqueous oxytocin solution at pH\* 3.5 and heptane containing 5% (w/w) of the nonionic emulgator sorbitan tristearate. A stable emulsion with mean droplet diameter of  $15\text{ }\mu\text{m}$  was obtained by pressing the mixture through a stainless steel mesh ( $20\text{ }\mu\text{m}$  pore size) 100 times as described previously.<sup>21</sup> The second MRD sample contained 32 mM oxytocin in a 52/48 (v/v) water/acetone cryosolvent at pH\* 3.4. The NOE sample contained 35 mM oxytocin in a 70/30 (v/v) water/acetone- $d_6$  cryosolvent at pH\* 3.4.

Bovine pancreatic trypsin inhibitor (BPTI), generously supplied by Novo Nordisk A/S (Gentofte, Denmark), was dialyzed against deionized, double-distilled water and then lyophilized. An aqueous BPTI solution of pH\* 5.2, made from water containing 52%  $^2\text{H}$  and 17%  $^{17}\text{O}$ , was mixed with an equal volume heptane/emulgator solution and emulsified as for the oxytocin sample. The BPTI concentration in the aqueous phase, 8.3 mM, was determined from the absorbance at 280 nm.

In an emulsion droplet of  $15\text{ }\mu\text{m}$  diameter, only 0.4% of the solute molecules (oxytocin or BPTI) are within  $100\text{ }\text{Å}$  of the interface. Any perturbation of the solute resulting from its interaction with the interface is therefore not likely to produce measurable effects. Indeed, no effect of the interface could be detected in a control experiment where the  $^2\text{H}$  dispersion profile from a 21 mM BPTI solution in  $\text{D}_2\text{O}$  at pH\* 5.3 and  $27\text{ }^\circ\text{C}$  was recorded with and without confinement to emulsion droplets.<sup>21</sup>

BPTI has recently been shown to self-associate into a specific decamer structure under a wide range of solution conditions.<sup>22,23</sup> Because of the stoichiometry, the fraction BPTI in decameric form depends strongly on the total BPTI concentration. Extrapolating from previous results at 14.4 mM BPTI and 4 or  $27\text{ }^\circ\text{C}$ ,<sup>23</sup> we expect the decamer fraction to be negligibly small at the BPTI concentration (8.3 mM) used for the present MRD experiments. Cold denaturation of BPTI in the deeply supercooled solutions investigated here is another potential concern.<sup>24</sup> However, BPTI is an exceptionally stable protein and extrapolation of the available thermodynamic data on BPTI unfolding<sup>25</sup> indicates that, even with the three disulfide bridges disrupted, cold denaturation should not occur above  $-100\text{ }^\circ\text{C}$ .

**2.2. MRD Experiments.** Magnetic relaxation dispersion (MRD) profiles of the water  $^2\text{H}$  and  $^{17}\text{O}$  longitudinal relaxation rate  $R_1 = 1/T_1$  were acquired at  $-25\text{ }^\circ\text{C}$  (oxytocin samples) or at  $-10$  and  $-30\text{ }^\circ\text{C}$  (BPTI samples). At  $-30\text{ }^\circ\text{C}$ , we only report  $^2\text{H}$  data because the short  $T_1$  severely reduced the  $^{17}\text{O}$  sensitivity. Each dispersion profile is based on relaxation experiments at 8–9 magnetic field strengths, accessed

- (9) Clore, G. M.; Bax, A.; Wingfield, P. T.; Gronenborn, A. M. *Biochemistry* **1990**, *29*, 5671–5676.
- (10) Wang, Y.-X.; Freedberg, D. I.; Grzesiek, S.; Torchia, D. A.; Wingfield, P. T.; Kaufman, J. D.; Stahl, S. J.; Chang, C.-H.; Hodge, C. N. *Biochemistry* **1996**, *35*, 12694–12704.
- (11) Otting, G.; Liepinsh, E.; Wüthrich, K. *Science* **1991**, *254*, 974–980.
- (12) Wüthrich, K.; Otting, G.; Liepinsh, E. *Faraday Discuss.* **1992**, *93*, 35–45.
- (13) Clore, G. M.; Bax, A.; Omichinski, J. G.; Gronenborn, A. M. *Structure* **1994**, *2*, 89–94.
- (14) Ernst, J. A.; Clubb, R. T.; Zhou, H. X.; Gronenborn, A. M.; Clore, G. M. *Science* **1995**, *267*, 1813–1817.
- (15) Halle, B. *J. Chem. Phys.* **2003**, *119*, 12372–12385.
- (16) Otting, G.; Liepinsh, E.; Farmer, B. T.; Wüthrich, K. *J. Biomol. NMR* **1991**, *1*, 209–215.
- (17) Brunne, R. M.; Liepinsh, E.; Otting, G.; Wüthrich, K.; van Gunsteren, W. F. *J. Mol. Biol.* **1993**, *231*, 1040–1048.

- (18) Otting, G.; Liepinsh, E.; Wüthrich, K. *J. Am. Chem. Soc.* **1992**, *114*, 4, 7093–7095.
- (19) Denisov, V. P.; Carlström, G.; Venu, K.; Halle, B. *J. Mol. Biol.* **1997**, *268*, 118–136.
- (20) Sunnerhagen, M.; Denisov, V. P.; Venu, K.; Bonvin, A. M. J. J.; Carey, J.; Halle, B.; Otting, B. *J. Mol. Biol.* **1998**, *282*, 847–858.
- (21) Jóhannesson, H.; Halle, B. *J. Am. Chem. Soc.* **1998**, *120*, 6859–6870.
- (22) Hamiaux, C.; Pérez, J.; Prangé, T.; Veessler, S.; Riès-Kautt, M.; Vachette, P. *J. Mol. Biol.* **2000**, *297*, 697–712.
- (23) Gottschalk, M.; Venu, K.; Halle, B. *Biophys. J.* **2003**, *84*, 3941–3958.
- (24) Privalov, P. L. *Crit. Rev. Biochem. Mol. Biol.* **1990**, *25*, 281–305.
- (25) Makhatadze, G. I.; Kim, K.-S.; Woodward, C.; Privalov, P. L. *Protein Sci.* **1993**, *2*, 2028–2036.

with a Varian 600 Unity Plus, Bruker Avance DMX 100 and 200 NMR spectrometers and a field-variable iron-core magnet (Drusch EAR-35N) equipped with a field-variable lock and flux stabilizer and interfaced to a modified Bruker MSL 100 console. The resonance frequency ranged from 2.5 to 92 MHz ( $^2\text{H}$ ) or from 2.2 to 81 MHz ( $^{17}\text{O}$ ). The sample temperature was adjusted with an accuracy of 0.1 °C by a thermostated flow of nitrogen gas and was checked with a copper–constantan thermocouple referenced to an ice bath. As a further temperature control, the field-independent  $T_1$  of a pure water reference sample (of the same isotope composition) was measured together with the oxytocin or BPTI sample at each field.

The relaxation time  $T_1$  was measured by the inversion recovery method, using a 16-step phase cycle, 20 evolution times in random order, and a sufficient number of transients to obtain a signal-to-noise ratio of at least 100. The accuracy of the reported  $R_1$  values is estimated to 0.5% (one standard deviation). The MRD profiles were analyzed with an in-house Matlab implementation of the Levenberg–Marquardt nonlinear  $\chi^2$  minimization algorithm.<sup>26</sup> To estimate the uncertainty in the fitted parameters, we performed fits on Monte Carlo generated ensembles of 1000 data sets, subject to random Gaussian noise with 0.5% standard deviation. Quoted uncertainties correspond to a confidence level of 68.3% (one standard deviation).

**2.3. NOE Experiments.** High-resolution intermolecular  $^1\text{H}$ – $^1\text{H}$  nuclear Overhauser effect (NOE) experiments were performed on a sample of oxytocin in a cryosolvent at  $-25$  °C using a Bruker DMX 600 spectrometer operating at a  $^1\text{H}$  resonance frequency of 600 MHz. The experiments used NOE-NOESY and ROE-NOESY pulse sequences<sup>27</sup> to study water–peptide  $^1\text{H}$ – $^1\text{H}$  cross-relaxation in the laboratory and rotating frames, respectively. In these experiments, the water magnetization is excited selectively, while the peptide resonances are defocused to avoid radiation damping or dipolar field artifacts.<sup>28</sup> During the following mixing time  $\tau_{\text{m1}}$ , water magnetization is transferred to the peptide resonances by NOE or ROE mixing. The rest of the pulse sequence is identical for the two experiments: peptide magnetization precesses during the evolution time  $t_1$  and is then transferred by intramolecular NOEs to other peptide resonances during the NOESY mixing time  $\tau_{\text{m2}}$ , whereupon diagonal peaks and cross-peaks are recorded during the detection period  $t_2$ . Further details about the pulse sequences can be found in the Supporting Information.

At the low temperature and high acetone concentration used, the labile protons of oxytocin exchange sufficiently slowly to yield resolved resonances. From the broadening of the large exchange peak in a ROESY spectrum, an exchange time of 8 ms was determined for the N-terminal ammonium protons. At such low exchange rates, exchange-relayed NOEs can be distinguished from direct NOEs with water by the slower build-up of the two-step magnetization transfer at short mixing times. Exchange-relayed NOEs, characterized by cross-peak intensities with  $|I_{\text{NOE}}/I_{\text{ROE}}| > 1$ , were thus observed for Cys-1  $\alpha\text{H}$  and  $\beta\text{H}$ , Tyr-2 NH (yields a direct exchange cross-peak at higher temperatures),  $\beta\text{H}$  and  $\epsilon\text{H}$ , and Cys-6  $\beta\text{H}$ .

For the short mixing times used in the oxytocin study ( $\tau_{\text{m1}} = 30$  and 15 ms, respectively), the intensities of the diagonal peaks in the NOE-NOESY and ROE-NOESY spectra are proportional to the cross-relaxation rates  $\sigma_{\text{L}}$  and  $\sigma_{\text{R}}$  in the laboratory and rotating frames, respectively. Intensities were measured on the cross-peaks whenever the diagonal peaks were unresolved. The ratio  $\sigma_{\text{L}}/\sigma_{\text{R}}$  of cross-relaxation rates was obtained from the corresponding ratio of peak intensities according to:

$$\frac{I_{\text{NOE}}}{I_{\text{ROE}}} = \frac{\sigma_{\text{L}} \tau_{\text{m1}}^{\text{NOE}}}{\sigma_{\text{R}} \tau_{\text{m1}}^{\text{ROE}}} = 2 \frac{\sigma_{\text{L}}}{\sigma_{\text{R}}} \quad (1)$$

### 3. Interpretation of NMR Data on Biomolecular Hydration

**3.1. Water  $^2\text{H}$  and  $^{17}\text{O}$  Quadrupolar Relaxation.** The relaxation dispersion,  $R_1(\omega_0)$ , of the quadrupolar water nuclei  $^2\text{H}$  and  $^{17}\text{O}$  is usually expressed in the form<sup>1,2</sup>

$$R_1(\omega_0) = R_{\text{bulk}} + 0.2J(\omega_0) + 0.8J(2\omega_0) \quad (2)$$

where  $R_{\text{bulk}}$  is the frequency-independent relaxation rate of the bulk solvent, measured separately on a reference sample, and  $\omega_0 = 2\pi \nu_0$  is the  $^2\text{H}$  or  $^{17}\text{O}$  resonance frequency in angular frequency units. All information about hydration is contained in the frequency-dependent quadrupolar spectral density,  $J(\omega_0)$ . In the simplest case, the observed frequency dependence of  $R_1$  within the experimentally accessible frequency window, typically 1–100 MHz, can be described by a single Lorentzian dispersion step. The spectral density function is then of the form

$$J(\omega) = \alpha + \beta \frac{\tau_{\beta}}{1 + (\omega\tau_{\beta})^2} \quad (3)$$

Sometimes, a second dispersion step is indicated at higher frequencies than the  $\beta$  dispersion. This so-called  $\gamma$  dispersion is described by a term like the  $\beta$  term in eq 3.

The model used to extract molecular-level information from the amplitude parameters  $\alpha$  and  $\beta$  and the correlation time  $\tau_{\beta}$  recognizes two classes of hydration water, both of which exchange rapidly (see below) with bulk water.  $N_{\alpha}$  water molecules have rotational correlation times  $\tau_{\alpha}$  that are significantly longer than the bulk water correlation time  $\tau_{\text{bulk}}$  but shorter than 1 ns. The effect of this class of perturbed water molecules is therefore to increase the relaxation rate  $R_1$  above the bulk water value  $R_{\text{bulk}}$  without producing a frequency dependence (dispersion) in  $R_1$  within the experimentally accessible range (<100 MHz). The effect of these water molecules is described by the parameter  $\alpha$ , which may be expressed as<sup>1,2</sup>

$$\alpha = \frac{R_{\text{bulk}}}{N_{\text{T}}} N_{\alpha} \left( \frac{\langle \tau_{\alpha} \rangle}{\tau_{\text{bulk}}} - 1 \right) \quad (4)$$

where  $N_{\text{T}}$  is the known water/biomolecule mole ratio. Previous MRD studies have shown that the  $\alpha$  contribution is produced by the water molecules in contact with the biomolecular surface. The number  $N_{\alpha}$  can therefore be estimated by dividing the solvent-accessible surface area of the peptide or protein by the mean area occupied by a water molecule at the surface. In eq 4,  $\langle \tau_{\alpha} \rangle$  is the mean rotational correlation time for the  $N_{\alpha}$  water molecules comprising the hydration layer.

For small solutes, the  $\alpha$  term fully accounts for the hydration effect on  $R_1$ . Biomolecules, on the other hand, usually contain a small number,  $N_{\beta}$ , of water molecules with sufficiently long (>1 ns) correlation times  $\tau_{\beta}$  to produce an observable frequency dependence in  $R_1$ . These few water molecules are responsible for the dispersive  $\beta$  term in eq 3, with<sup>1,2</sup>

$$\beta = \frac{\omega_{\text{Q}}^2}{N_{\text{T}}} N_{\beta} S_{\beta}^2 \quad (5)$$

(26) Press, W. H.; Teukolsky, S. A.; Vetterling, W. T.; Flannery, B. P. *Numerical Recipes in C*, 2nd ed.; Cambridge University Press: Cambridge, 1992.

(27) Liepinsh, E.; Otting, G. *J. Biomol. NMR* **1999**, *13*, 73–76.

(28) Sobol, A. G.; Wider, G.; Iwai, H.; Wüthrich, K. *J. Magn. Reson.* **1998**, *130*, 262–271.

**Table 1.** Parameter Values Used To Analyze MRD Data

parameter	symbol (unit)	value for	
		oxytocin <sup>a</sup>	BPTI <sup>b</sup>
water/biomolecule mole ratio	$N_T$ (-)	1350/910	6400
number of surface water molecules <sup>c</sup>	$N_\alpha$ (-)	73	268
biomolecule rotational correlation time <sup>d</sup>	$\tau_R$ (ns)	13/19	14/70

<sup>a</sup> The first value refers to pure water, and the second value refers to water/acetone cryosolvent, both at  $-25$  °C. <sup>b</sup> The first value refers to  $-10$  °C, the second value refers to  $-30$  °C. <sup>c</sup> Obtained by dividing the solvent-accessible ( $1.4$  Å probe radius) surface area of oxytocin (crystal structure IXY1<sup>29</sup>) or BPTI (crystal structure 5PTI<sup>29</sup>) by  $15$  Å<sup>2</sup>. <sup>d</sup> Obtained as described in the Supporting Information. For oxytocin,  $\tau_R$  is not needed to analyze the MRD data.

Here,  $\omega_Q$  is the rigid-lattice quadrupole coupling frequency:  $8.70 \times 10^5$  rad s<sup>-1</sup> for <sup>2</sup>H and  $7.61 \times 10^6$  rad s<sup>-1</sup> for <sup>17</sup>O.<sup>1,2</sup> Previous MRD studies have shown that only water molecules buried in internal cavities or in deep surface pockets have correlation times exceeding 1 ns (at room temperature). Such internal water molecules are usually strongly hydrogen-bonded to the protein, and their highly restricted rotational motions give rise to an orientational order parameter  $S_\beta$  that is usually not far below the rigid-binding limit of unity. Complete orientational randomization of internal water molecules takes place by either (or both) of two independent processes: rotational diffusion of the biomolecule, with rotational correlation time  $\tau_R$ , or exchange with bulk water, with mean residence time  $\tau_W$  in the internal hydration site. The correlation time  $\tau_\beta$  in eq 3 is therefore determined by<sup>1,2</sup>

$$\frac{1}{\tau_\beta} = \frac{1}{\tau_W} + \frac{1}{\tau_R} \quad (6)$$

The values of  $\tau_R$ ,  $N_\alpha$ , and  $N_T$  for the investigated NMR samples are collected in Table 1.

A water molecule contributes fully to the observed MRD profile, with amplitude and correlation time as given by eqs 5 and 6, only if it exchanges with bulk water at a rate much higher than the local spin relaxation rate in the hydration site.<sup>1,2</sup> Even when this fast-exchange condition is not satisfied, the MRD profile can still be described by eqs 2 and 3, but with apparent parameters  $\tau_{\beta,\text{app}}$  and  $(N_\beta S_\beta^2)_{\text{app}}$  related to the corresponding parameters in eqs 5 and 6 as described in the Supporting Information.

**3.2. Biomolecule–Water <sup>1</sup>H–<sup>1</sup>H Cross-Relaxation.** The laboratory and rotating frame cross-relaxation rates appearing in eq 1 are governed by the reduced dipolar spectral density function  $j(\omega)$  according to<sup>31</sup>

$$\sigma_L(\omega_0) = K[0.6j(2\omega_0) - 0.1j(0)] \quad (7a)$$

$$\sigma_R(\omega_0) = K[0.3j(\omega_0) + 0.2j(0)] \quad (7b)$$

where  $K = [(\mu_0/4\pi)\hbar\gamma^2]^2 = 5.695 \times 10^{11}$  Å<sup>6</sup> s<sup>-2</sup>. Because  $j(\omega)$  is a monotonically decreasing function, it follows that the ratio  $\sigma_L/\sigma_R$  can vary from  $+1$  to  $-0.5$ . The limit  $\sigma_L/\sigma_R = 1$  corresponds to fast dynamics with  $j(0) = j(\omega_0) = j(2\omega_0)$ ,

whereas the limit  $\sigma_L/\sigma_R = -0.5$  corresponds to slow dynamics with  $j(0) \gg j(\omega_0) > j(2\omega_0)$ . Here, “fast” and “slow” should be understood in relation to  $1/\omega_0 \approx 300$  ps (for a <sup>1</sup>H resonance frequency of 600 MHz).

NOE data acquired at a single frequency are not as readily interpreted as MRD data covering a wide frequency range. In particular, the separation of the strength of the dipole–dipole couplings, involving the number of interacting water protons and their distances from a particular biomolecular proton, from the rate of modulation of the dipole–dipole vectors, containing the desired information about hydration dynamics, is highly model-dependent.<sup>4,32,33</sup> For a pair of protons at fixed separation  $r_{\text{HH}}$ , rigidly attached to a solute that tumbles isotropically with rotational correlation time  $\tau_R$ , the dipolar spectral density function is<sup>34</sup>

$$j(\omega) = \frac{1}{r_{\text{HH}}^6} \frac{\tau_R}{1 + (\omega\tau_R)^2} \quad (8)$$

An expression like this, but with  $\tau_R$  replaced by an effective correlation time as in eq 6, may be a reasonable approximation for an NOE with a long-lived water molecule trapped in a cavity or deep crevice.<sup>19</sup>

When applied to surface hydration, the intramolecular spectral density in eq 8 has two major shortcomings: it only takes into account a single pair of protons, and it neglects their relative translational motion. Because only one water <sup>1</sup>H resonance is observed, the measured cross-relaxation rates are, in principle, affected by dipole–dipole couplings between a particular biomolecule proton and all water protons in the sample. Although the square of the dipole–dipole coupling falls off with distance as  $r^{-6}$  (as in eq 8), the number of water protons at a given distance increases as  $r^2$  and the characteristic time for angular modulation of the proton–proton vector by water translational diffusion also increases as  $r^2$ . On integrating the resulting  $r^{-2}$  dependent product of these factors from  $r = d$  (the distance of closest approach) to infinity, one recovers the well-known<sup>34</sup>  $1/d$  scaling of  $j(0)$ . Because the contribution from solvent protons at separation  $r$  falls off as  $r^{-2}$  (rather than  $r^{-6}$ ), cross-relaxation between water and biomolecular protons does not in general reflect local hydration dynamics, but is dominated by long-range dipole–dipole couplings with bulk water.<sup>15</sup>

In the past, water–biomolecule NOEs have been interpreted either with the intramolecular spectral density in eq 8 (or a variant that takes internal motions into account) or with an intermolecular spectral density based on a model where the dipole-coupled water and biomolecule protons reside in spherical particles undergoing translational and rotational diffusion.<sup>32</sup> If the water protons are placed at the center of the water sphere, which is an excellent approximation due to the fast water rotation, water dynamics enters the model solely via the water translational diffusion coefficient  $D$ . For given values of the other model parameters, a measured  $\sigma_L/\sigma_R$  ratio can thus be transformed into a water diffusion coefficient.<sup>3,4,11</sup> In previous NOE studies, it has invariably been assumed (explicitly or implicitly) that the cross-relaxation rates involve only one or a few water molecules in the immediate vicinity of the observed

(29) Wood, S. P.; Tickle, I. J.; Trehanne, A. M.; Pitts, J. E.; Mascarenhas, Y.; Li, J. Y.; Husain, J.; Cooper, S.; Blundell, T. L.; Hruby, V. J.; Buku, A.; Fischman, A. J.; Wyssbrod, H. R. *Science* **1986**, *232*, 633–636.

(30) Wlodawer, A.; Walter, J.; Huber, R.; Sjölin, L. *J. Mol. Biol.* **1984**, *180*, 301–329.

(31) Neuhaus, D.; Williamson, M. P. *The Nuclear Overhauser Effect in Structural and Conformational Analysis*, 2nd ed.; Wiley-VCH: New York, 2000.

(32) Ayant, Y.; Belorizky, E.; Fries, P.; Rosset, J. *J. Phys.* **1977**, *38*, 325–337.

(33) Brüschweiler, R.; Wright, P. E. *Chem Phys. Lett.* **1994**, *229*, 75–81.

(34) Abragam, A. *The Principles of Nuclear Magnetism*; Clarendon Press: Oxford, 1961; Chapter VIII E (c).

**Table 2.** Parameter Values Used with the Nonuniform Diffusion Model

parameter	symbol (unit)	value for	
		oxytocin <sup>a</sup>	BPTI <sup>b</sup>
solvent-accessible biomolecule radius	$b$ (Å)	10	15
minimum distance of closest approach	$d$ (Å)	2.5	2.5
thickness of hydration layer	$\delta$ (Å)	1.5	2.4
biomolecule rotational correlation time	$\tau_R$ (ns)	13.5	6.7
bulk water diffusion coefficient	$D_{\text{bulk}}$ ( $10^{-9}$ m <sup>2</sup> s <sup>-1</sup> )	0.24	1.2
translational retardation factor	$D_{\text{bulk}}/D_{\text{hyd}}$ (-)	3 <sup>c</sup>	2 <sup>c</sup>
water proton number density	$n_H$ (nm <sup>-3</sup> )	47	67
<sup>1</sup> H resonance frequency	$\nu_0$ (MHz)	600	500

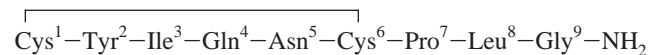
<sup>a</sup> In water/acetone cryosolvent at -25 °C. <sup>b</sup> In water at 4 °C. <sup>c</sup> Values estimated from MRD results.

biomolecular proton. However, if the cross-relaxation rates are dominated by long-range dipole–dipole couplings, the diffusion coefficient  $D$  deduced from the model mainly reflects the dynamics of bulk water.

To characterize the perturbation of water dynamics by the biomolecule, that is, the hydration dynamics, a more general model is needed that allows the water diffusion coefficient to take different values in the hydration layer ( $D_{\text{hyd}}$ ) and in the bulk solvent ( $D_{\text{bulk}}$ ). An analytical spectral density function for such a nonuniform diffusion model has recently been derived.<sup>15</sup> The model describes the peptide or protein as a sphere covered by a hydration layer with reduced water diffusion coefficient  $D_{\text{hyd}}$ . In our calculations, the thickness  $\delta$  of this hydration layer is determined by the condition that the volume of the spherical shell equals the volume occupied by a monolayer of  $N_\alpha$  water molecules on the real (nonspherical) protein surface. Because water translation and rotation are both rate-limited by hydrogen-bond dynamics,<sup>7,35</sup> the translational retardation factor  $D_{\text{bulk}}/D_{\text{hyd}}$  that enters the nonuniform diffusion model can be set equal to the rotational retardation factor  $\langle\tau_\alpha\rangle/\tau_{\text{bulk}}$  deduced from MRD data by means of eq 4. Unlike previous models, the nonuniform diffusion model allows NOE and MRD data to be interpreted within the same theoretical framework. The parameter values used in applying the nonuniform diffusion model to NOE data for oxytocin and BPTI are collected in Table 2 and are rationalized in the Supporting Information.

#### 4. Oxytocin Hydration

Oxytocin, a neurohypophyseal hormone, is a cyclic nonapeptide with amidated C-terminus:<sup>36</sup>



An early double-resonance NMR study<sup>37</sup> demonstrated saturation transfer from water protons to oxytocin protons at 30 °C. In difference spectra, with and without saturation of the water resonance, negative peaks were seen for labile NH protons exchanging with water protons on the millisecond–second time scale, while positive peaks were observed for solvent-exposed nonlabile CH protons experiencing a positive NOE with water, the positive sign being attributed to the short (subnanosecond)

correlation time for the intermolecular dipole coupling.<sup>37</sup> In that study, solvent magnetization transfer was used primarily to elucidate the solution conformation of the peptide rather than for studying solvation per se. More recently, 2D NOESY and ROESY spectra of 50 mM oxytocin in water at 6 °C were shown to exhibit cross-peaks between water and all observed oxytocin resonances.<sup>11</sup> The reported  $\sigma_L/\sigma_R$  ratios in the range 0.3–0.5 were taken to imply residence times in the range 100–250 ps for the water molecules in contact with oxytocin. In a subsequent 2D NOESY/ROESY study of oxytocin hydration,<sup>18</sup> where temperatures down to -25 °C were reached with the aid of a water/acetone cryosolvent, a sign reversal of  $\sigma_L$  was observed for all resonances between 0 and -15 °C. This result was taken to imply water residence times of about 500 ps at the temperature of zero-crossing and, by implication, considerably longer residence times at -25 °C. Because water residence times of several nanoseconds should be directly observable in the water <sup>2</sup>H and <sup>17</sup>O relaxation dispersion, we decided to examine the hydration dynamics of oxytocin at -25 °C by MRD.

**4.1. MRD Results.** We measured the longitudinal relaxation rate  $R_1$  of the water <sup>2</sup>H and <sup>17</sup>O magnetizations as a function of the resonance frequency  $\nu_0$  in two oxytocin samples at -25 °C. In one sample, oxytocin was dissolved in a water/acetone cryosolvent as in the NOE study. In the other sample, the same temperature could be reached without a cryosolvent by dispersing the aqueous oxytocin solution in 15  $\mu$ m diameter emulsion droplets, thereby inhibiting the heterogeneous nucleation process that causes water to freeze at or near 0 °C.<sup>38</sup> This sample gives a more clear-cut picture of hydration dynamics, without the complication of preferential solvation in the mixed cryosolvent.

With an estimated rotational correlation time  $\tau_R$  of 13 ns for oxytocin (Table 1) and a residence time  $\tau_W$  of several nanoseconds for most hydration sites,<sup>18</sup> a substantial dispersion is expected (see eq 6). However, no frequency dependence can be seen in the <sup>2</sup>H MRD data up to 30 MHz (Figure 1). The average rotational retardation in the hydration layer can be obtained from the average relative relaxation rate  $\langle R_1/R_{\text{bulk}} \rangle$ . From eq 4, with  $\alpha/R_{\text{bulk}} = \langle R_1/R_{\text{bulk}} \rangle - 1$  and  $N_\alpha/N_T = 0.054$  (Table 1), we obtain a rotational retardation factor  $\langle\tau_\alpha\rangle/\tau_{\text{bulk}} = 3.3 \pm 0.2$ . With  $\tau_{\text{bulk}} \approx 17$  ps,<sup>39</sup> this corresponds to  $\langle\tau_\alpha\rangle \approx 55$  ps. In bulk water, the mean time taken to diffuse one molecular diameter is close to the rank-1 rotational correlation time (related to the Legendre polynomial  $P_1(\cos \theta)$ ), that is, 3 times the rank-2 correlation time (related to  $P_2(\cos \theta)$ ) measured by NMR.<sup>34</sup> Accordingly, we estimate the average residence time of water molecules in the hydration layer of oxytocin as 165 ps at -25 °C, an order of magnitude less than suggested by the NOE study.<sup>18</sup>

To examine the effect of acetone on the hydration dynamics, we also performed MRD experiments on a sample of oxytocin dissolved in a water/acetone cryosolvent. As seen from the <sup>2</sup>H MRD data in Figure 1b, there is still no sign of a relaxation dispersion. For this sample, with  $N_\alpha/N_T = 0.080$  (Table 1), we obtain  $\langle\tau_\alpha\rangle/\tau_{\text{bulk}} = 2.4 \pm 0.1$ , significantly less than for the emulsified sample without acetone in the solvent. This does not mean that the hydration water is more mobile in the cryosolvent sample, because the presence of acetone in the bulk solvent

(35) Marchi, M.; Sterpone, F.; Ceccarelli, M. *J. Am. Chem. Soc.* **2002**, *124*, 6787–6791.

(36) Hruby, V. J. In *Topics in Molecular Pharmacology*; Burgen, A. S. V., Roberts, G. C. K., Eds.; Elsevier/North-Holland: Amsterdam, 1981; pp 99–126.

(37) Glickson, J. D.; Rowan, R.; Pitner, T. P.; Dadok, J.; Bothner-By, A. A.; Walter, R. *Biochemistry* **1976**, *15*, 1111–1119.

(38) Rasmussen, D. H.; Mackenzie, A. P. In *Water Structure at the Water–Polymer Interface*; Jellinek, H. H. G., Ed.; Plenum: New York, 1972; pp 126–145.

(39) Modig, K.; Halle, B. *J. Am. Chem. Soc.* **2002**, *124*, 12031–12041.

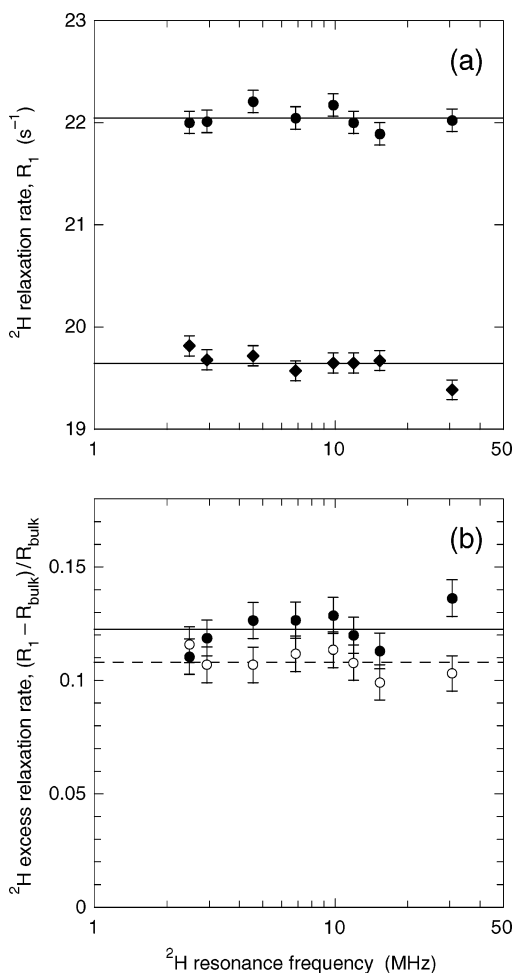


**Figure 1.** (a) Water  $^2\text{H}$  relaxation rate versus resonance frequency for an emulsified aqueous solution of 41 mM oxytocin at  $\text{pH}^* 3.5$  and  $-25\text{ }^\circ\text{C}$  (●) and for the bulk solvent (50/50  $\text{H}_2\text{O}/\text{D}_2\text{O}$ ) at the same temperature (○). The lines represent averages of the data points shown. (b) Comparison of the  $^2\text{H}$  relaxation data (●, solid line) in subfigure (a) with data from a solution of 32 mM oxytocin in a 52/48 (v/v) water/acetone cryosolvent at  $\text{pH}^* 3.4$  and  $-25\text{ }^\circ\text{C}$  (○, dashed line). To remove the trivial effect of acetone on the bulk solvent relaxation rate, the data have been normalized by  $R_{\text{bulk}}$  (Table 3).

**Table 3.** MRD Results for Oxytocin at  $-25\text{ }^\circ\text{C}$

sample	nucleus	$R_{\text{bulk}}$ ( $\text{s}^{-1}$ )	$\langle R_1/R_{\text{bulk}} \rangle - 1$	$\langle \tau_\alpha \rangle / \tau_{\text{bulk}}^a$
emulsion	$^2\text{H}$	19.6	$0.12 \pm 0.01$	$3.3 \pm 0.2$
emulsion	$^{17}\text{O}$	1510	$0.14 \pm 0.03$	$3.6 \pm 0.5$
cryosolvent	$^2\text{H}$	34.8	$0.11 \pm 0.01$	$2.4 \pm 0.1$
cryosolvent	$^{17}\text{O}$	2610	$0.12 \pm 0.01$	$2.4 \pm 0.1$

<sup>a</sup> Calculated from eq 4 with  $N_\alpha = 73$ .

increases  $\tau_{\text{bulk}}$ . Noting that  $\tau_{\text{bulk}}$  is proportional to  $R_{\text{bulk}}$ , we can use the  $R_{\text{bulk}}$  values measured for the two solvents (Table 3) to normalize to the pure water reference state. We thus find  $\langle \tau_\alpha \rangle / \tau_{\text{bulk}}^0 = 4.2 \pm 0.1$  for the cryosolvent sample. Here,  $\tau_{\text{bulk}}^0$  refers to pure water (as in the emulsion sample), while  $\langle \tau_\alpha \rangle$  refers to the hydration layer of oxytocin in the cryosolvent. Furthermore, if some of the water molecules in the hydration layer are displaced by acetone molecules,  $N_\alpha$  should be smaller than 73. For example, if  $N_\alpha$  is reduced by 30%, our estimate of  $\langle \tau_\alpha \rangle / \tau_{\text{bulk}}^0$  increases from 4.2 to 5.6 (see eq 4). In any case, the effect of acetone on the hydration dynamics is modest, whether it is a direct consequence of water–acetone interactions in the hydration layer or an indirect effect of an altered oxytocin

conformation in the cryosolvent. The inconsistency with the NOE study<sup>18</sup> thus remains.

The  $^{17}\text{O}$  MRD data acquired for the two samples (not shown), although less complete (3–7 frequencies) and with more scatter (due to signal loss during the receiver dead-time for the rapidly relaxing  $^{17}\text{O}$  magnetization), are fully consistent with the  $^2\text{H}$  data (Table 3). The near coincidence of the normalized  $^2\text{H}$  and  $^{17}\text{O}$  rates indicates that the labile oxytocin hydrogens (N-terminal  $\text{NH}_3$  and Tyr-2 OH) exchange too slowly with water at  $-25\text{ }^\circ\text{C}$  to contribute significantly to the  $^2\text{H}$  relaxation. Indeed, the intrinsic  $^2\text{H}$  relaxation time of these labile deuterons is estimated to a few  $100\text{ }\mu\text{s}$ , 2 orders of magnitude shorter than the exchange times implied by line broadening in a ROESY spectrum (section 2.3).

**4.2. NOE Results.** To allow a more detailed comparison of MRD and NOE data, we recorded new NOE data for oxytocin in a water/acetone cryosolvent at  $-25\text{ }^\circ\text{C}$ . The oxytocin preparation was the same as used for the MRD study. For these experiments, we used NOE-NOESY and ROE-NOESY schemes<sup>27</sup> that improve the sensitivity and reduce artifacts as compared to the original low-temperature NOE study of oxytocin.<sup>18</sup> Diagonal cross sections through the  $^1\text{H}$ – $^1\text{H}$  NOE-NOESY and ROE-NOESY spectra, showing the intermolecular water–oxytocin NOEs, are displayed in Figure 2. Exchange cross-peaks with water were observed for Cys-1  $\alpha\text{NH}_3$  and Tyr-2 OH. With protons showing NOEs to these labile protons excluded,  $\sigma_L/\sigma_R$  ratios from 34 direct oxytocin–water NOE cross-peaks were obtained with the aid of eq 1. All ratios are negative, and some are at, or near, the slow motion limit of  $-0.5$  (Table 4).

According to eqs 6–8, with  $\nu_0 = 600\text{ MHz}$  and  $\tau_R = 13.5\text{ ns}$  (Table 2),  $\sigma_L/\sigma_R$  values between 0 and  $-0.4$  correspond to water residence times  $\tau_W$  between 0.3 and 1.0 ns, whereas  $\sigma_L/\sigma_R$  values between  $-0.4$  and  $-0.5$  correspond to  $\tau_W$  values longer than 1 ns. Such an interpretation of the NOE data in Table 4 is not consistent with the MRD results in Figure 1. Because the crystal structure of oxytocin<sup>29</sup> does not reveal hydration sites in cavities or deep pockets, the intramolecular spectral density in eq 8 is not appropriate. We therefore turn to the nonuniform diffusion model (section 3.2).

For the model calculations, we used the parameter values in Table 2 (see also the Supporting Information). For consistency with the MRD results (Table 3), we take  $D_{\text{bulk}}/D_{\text{hyd}} = 3$ , somewhat higher than the MRD value to account for the lower acetone concentration in the cryosolvent used for the NOE experiments. Furthermore, the thickness of the hydration layer (where the centers of the perturbed water molecules are found) is taken to be  $\delta = 1.5\text{ \AA}$ , corresponding to the same number ( $N_\alpha = 73$ ) of water molecules in contact with oxytocin as we used for the MRD analysis. Comparing the experimental and calculated  $\sigma_L/\sigma_R$  ratios (Table 4), we conclude that the nonuniform diffusion model rationalizes the NOE data remarkably well. The calculated  $\sigma_L/\sigma_R$  ratios are in the same range (from  $-0.44$  to  $-0.06$ ) as the experimental ratios (from  $-0.50$  to  $-0.03$ ). The mean value for the 34  $\sigma_L/\sigma_R$  ratios is  $-0.31$  (experimental) versus  $-0.22$  (calculated). Moreover, the variation in  $\sigma_L/\sigma_R$  among different oxytocin protons shows a modest correlation between experiment and model calculation ( $r = 0.67$ ). Because oxytocin in solution assumes a range of conformations<sup>40</sup> that are not necessarily similar to the crystal structure, the correlation between experimental and calculated  $\sigma_L/\sigma_R$  ratios, and its

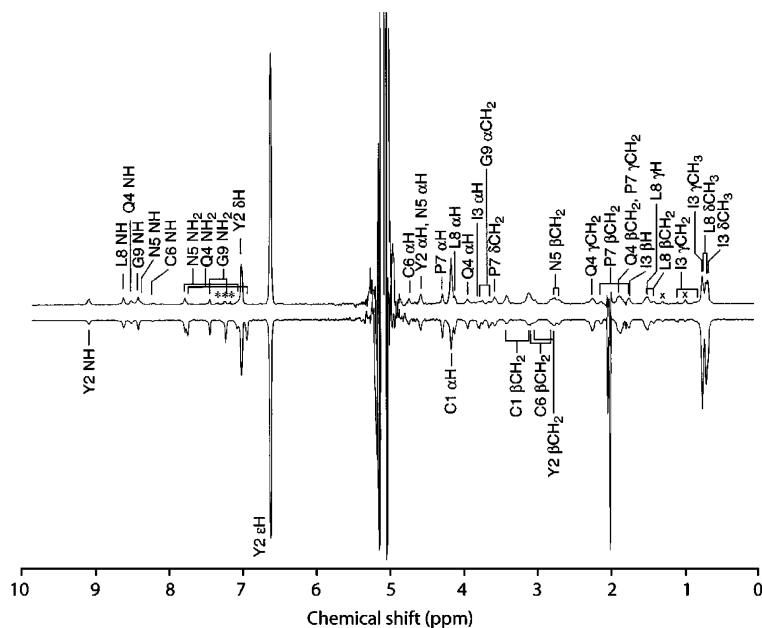


**Figure 2.** Diagonal cross sections through NOE-NOESY (upper) and ROE-NOESY (lower) spectra from a sample of 35 mM oxytocin in a 70/30 (v/v) water/acetone- $d_6$  cryosolvent at pH\* 3.4 and  $-25$  °C. The  $^1\text{H}$  resonance frequency was 600 MHz. Resonance assignments above the spectra refer to direct water–oxytocin NOEs, while those below the spectra identify intramolecular NOEs to exchanging oxytocin protons or direct exchange peaks. Asterisks and crosses label exchange peaks from ammonium and resonances from unidentified impurities, respectively.

physical origin, is brought out more clearly by identifying two extreme categories of oxytocin protons (labeled C and P in Table 4). These categories comprise, respectively, backbone atoms (likely to be protected from solvent access in most conformations) and side-chain atoms or atoms near the C-terminus (likely to be solvent exposed).

The core protons are defined as the 10 cross-peaks with the most negative ( $\leq -0.34$ )  $\sigma_L/\sigma_R$  ratios calculated on the basis of the crystal structure. Eight of these are also among the 10 most negative ( $\leq -0.38$ ) experimental  $\sigma_L/\sigma_R$  ratios. Moreover, the 10 core resonances have the smallest calculated  $\sigma_R$  rates (Table 4), and, consistently, all yield weak ROE cross-peaks (Figure 2). The peripheral protons are defined as the 10 cross-peaks with the least negative ( $\geq -0.08$ ) calculated  $\sigma_L/\sigma_R$  ratios. Seven of these are also among the 10 least negative ( $\geq -0.23$ ) experimental  $\sigma_L/\sigma_R$  ratios. Moreover, the 10 peripheral resonances have the largest calculated  $\sigma_R$  values (Table 4) and, consistently, 9 out of 10 yield intense ROE cross-peaks (Figure 2). (As expected, the most intense ROE cross-peaks within this category involve three-fold degenerate methyl protons.) In the calculation, the different oxytocin protons differ only in the distance of closest approach to water protons, which is 5–8 Å for the core resonances and the minimum 2.5 Å for the peripheral resonances. As expected, the distance of closest approach is correlated with the solvent-accessible area,  $A_S$ , of the heavy atoms bearing the protons (Table 4). We find  $\langle A_S \rangle = 8$  Å<sup>2</sup> for the core resonances and 44 Å<sup>2</sup> for the peripheral resonances. More importantly, the strong correlation between calculated and measured results for the two categories of oxytocin protons indicates that the NOE data report primarily on solvent exposure, rather than on hydration dynamics. A similar conclusion was drawn on the basis of a theoretical analysis of simplified models.<sup>33</sup>

Further insights into the physical origin of the NOE results are provided by the model calculations reported in Figure 3. Figure 3a and b demonstrates that the ratio  $\sigma_L/\sigma_R$  depends much more on the distance of closest approach,  $d$ , between a peptide proton and water protons (which, in a real biomolecule, is closely related to solvent exposure) than on hydration dynamics (via  $D_{\text{bulk}}/D_{\text{hyd}}$ ). While the model calculations in Table 4 used a value  $D_{\text{bulk}}/D_{\text{hyd}} = 3$  derived from the MRD data, the retardation of water diffusion in the hydration layer has a negligible effect on the observed cross-peak intensities. For the 34 oxytocin resonances, the difference between no dynamic perturbation at all ( $D_{\text{hyd}} = D_{\text{bulk}}$ ) and a rather large perturbation with  $D_{\text{bulk}}/D_{\text{hyd}} = 5$  is merely to change  $\langle \sigma_L/\sigma_R \rangle$  from  $-0.20$  to  $-0.24$ .

The insensitivity of  $\sigma_L/\sigma_R$  to the water diffusion coefficient in the hydration layer indicates that the cross-relaxation rates are dominated by bulk water. Contributions from water molecules at different distances from the oxytocin surface can be assessed by imposing an absorption boundary condition at a variable distance outside the surface.<sup>15</sup> We thus find that the  $\sigma_L/\sigma_R$  ratio converges very slowly for both core and peripheral resonances (Figure 3c). Whereas the first few water layers give positive contributions to  $\sigma_L/\sigma_R$ , it is the thousands of more remote water molecules that produce the negative  $\sigma_L/\sigma_R$  ratios that we observe. The physical origin of this behavior is that the orientation of a longer proton–proton vector is modulated more slowly because a water molecule must then diffuse a larger distance to sample a given solid angle. The motional “correlation times” probed by the NOE method are thus governed more by the spatial location of water molecules than by their mobilities. The difference between core and peripheral resonances is that the exclusion of water molecules from the vicinity of core protons makes the slowly modulated long-range dipole–dipole couplings to bulk water even more dominant than for peripheral protons.

(40) Glickson, J. D. In *Peptides: Chemistry, Structure, Biology*; Walter, R., Meisenhofer, J., Eds.; Ann Arbor Science: Ann Arbor, MI, 1975; pp 787–802.

**Table 4.** NOE Results for Oxytocin at  $-25\text{ }^{\circ}\text{C}$ 

residue	proton <sup>a</sup>	$\sigma_L/\sigma_R$		$\sigma_R^b$ ( $\text{s}^{-1}$ )	$d^c$ ( $\text{\AA}$ )	$A_S^d$ ( $\text{\AA}^2$ )	category <sup>e</sup>
		exp't	theory <sup>b</sup>				
Tyr-2	$\alpha\text{H}$ (1)	-0.50	-0.36	0.06	5.1	12	C
Tyr-2	$\delta\text{H}$ (2)	-0.33	-0.20	0.09	4.1	13	
Ile-3	$\alpha\text{H}$ (1)	-0.50	-0.34	0.07	4.8	5	C
Ile-3	$\beta\text{H}$ (1)	-0.50	-0.12	0.12	2.8	11	
Ile-3	$\gamma^1\text{H}$ (2)	-0.33	-0.09	0.13	2.6	36	
Ile-3	$\gamma^2\text{H}$ (3)	-0.33	-0.06	0.14	2.5	40	P
Ile-3	$\delta\text{H}$ (3)	-0.26	-0.08	0.13	2.6	66	P
Gln-4	NH (1)	-0.50	-0.37	0.06	5.2	3	C
Gln-4	$\alpha\text{H}$ (1)	-0.26	-0.36	0.06	5.0	9	C
Gln-4	$\beta\text{H}$ (2)	-0.36	-0.19	0.10	3.2	23	
Gln-4	$\gamma\text{H}$ (2)	-0.23	-0.08	0.13	2.6	30	P
Gln-4	$\epsilon\text{NH}^1$ (1) <sup>f</sup>	-0.07	-0.06	0.14	2.5	47	P
Gln-4	$\epsilon\text{NH}^2$ (1) <sup>f</sup>	-0.03	-0.06	0.14	2.5	47	P
Asn-5	$\alpha\text{H}$ (1)	-0.36	-0.41	0.05	6.5	8	C
Asn-5	$\beta\text{H}$ (2)	-0.50	-0.38	0.06	5.6	21	C
Asn-5	$\delta\text{NH}^1$ (1) <sup>f</sup>	-0.24	-0.31	0.07	4.3	31	
Asn-5	$\delta\text{NH}^2$ (1) <sup>f</sup>	-0.12	-0.29	0.08	4.0	31	
Cys-6	NH (1)	-0.42	-0.43	0.05	7.6	4	C
Cys-6	$\alpha\text{H}$ (1)	-0.50	-0.44	0.05	8.0	0	C
Pro-7	$\alpha\text{H}$ (1)	-0.28	-0.32	0.07	4.4	15	
Pro-7	$\beta\text{H}^1$ (1) <sup>f</sup>	-0.23	-0.12	0.12	2.8	41	
Pro-7	$\beta\text{H}^2$ (1) <sup>f</sup>	-0.29	-0.23	0.09	3.5	41	
Pro-7	$\gamma\text{H}$ (2)	-0.29	-0.27	0.08	3.8	34	
Pro-7	$\delta\text{H}$ (2)	-0.50	-0.40	0.06	5.9	13	C
Leu-8	NH (1)	-0.46	-0.35	0.06	4.9	0	C
Leu-8	$\alpha\text{H}$ (1)	-0.29	-0.06	0.14	2.5	4	P
Leu-8	$\beta\text{H}$ (2)	-0.33 <sup>g</sup>	-0.14	0.11	3.1	15	
Leu-8	$\gamma\text{H}$ (1)	-0.33 <sup>g</sup>	-0.23	0.09	3.5	2	
Leu-8	$\delta^1\text{H}$ (3)	-0.16	-0.10	0.12	2.7	55	
Leu-8	$\delta^2\text{H}$ (3)	-0.17	-0.06	0.14	2.5	60	P
Gly-9	NH (1)	-0.38	-0.32	0.07	4.4	0	
Gly-9	$\alpha\text{H}$ (2)	-0.14	-0.06	0.14	2.5	45	P
Gly-9	NH <sup>1</sup> (1) <sup>f</sup>	-0.17	-0.08	0.13	2.6	51	P
Gly-9	NH <sup>2</sup> (1) <sup>f</sup>	-0.07	-0.06	0.14	2.5	51	P

<sup>a</sup> Number of contributing protons given within parentheses. <sup>b</sup> Calculated from the nonuniform diffusion model with parameter values from Table 2. When more than one peptide proton is involved, the cross-relaxation rates were calculated as averages over the individual protons. <sup>c</sup> Distance of closest approach between oxytocin and water protons. When more than one peptide proton is involved, the average  $d$  value is given. <sup>d</sup> Solvent-accessible area for the associated heavy atom, computed with a probe radius of 1.4  $\text{\AA}$ . For cross-peaks involving protons bound to more than one heavy atom, the average  $A_S$  is given. <sup>e</sup> Oxytocin proton categories, core (C) and peripheral (P), as defined in the text. <sup>f</sup> For nondegenerate geminal protons, superscripts 1 and 2 refer to the low-field and high-field resonances, respectively. For the amide groups, the low-field resonance was assigned to the trans proton with respect to the carbonyl oxygen. <sup>g</sup> Overlap between the Leu-8  $\gamma\text{H}$  and low-field  $\beta\text{H}$  resonances.

In the conventional analysis, the more negative  $\sigma_L/\sigma_R$  ratios for the core resonances would be interpreted as evidence for longer residence times for water molecules that penetrate more deeply into the oxytocin structure. However, the core resonances should then have the most intense ROE cross-peaks ( $\sigma_R$  increases monotonically with increasing correlation time), contrary to what is observed. Figure 3d shows the effect on  $\sigma_L/\sigma_R$  of including a single site-bound water molecule with residence time  $\tau_W$  and with the two water protons just 3  $\text{\AA}$  from the reference oxytocin proton. Note that, while mobile and site-bound water molecules contribute additively to  $\sigma_L$  and  $\sigma_R$ , this is not the case for the ratio  $\sigma_L/\sigma_R$ . The counterintuitive increase of  $\sigma_L/\sigma_R$  with  $\tau_W$  for  $\tau_W < 100$  ps occurs because such water exchange dynamics are faster than the modulation of the dominant bulk water dipole couplings.

## 5. BPTI Hydration

BPTI has served as testing ground for the development of both the MRD and the NOE methods. The crystal structure of

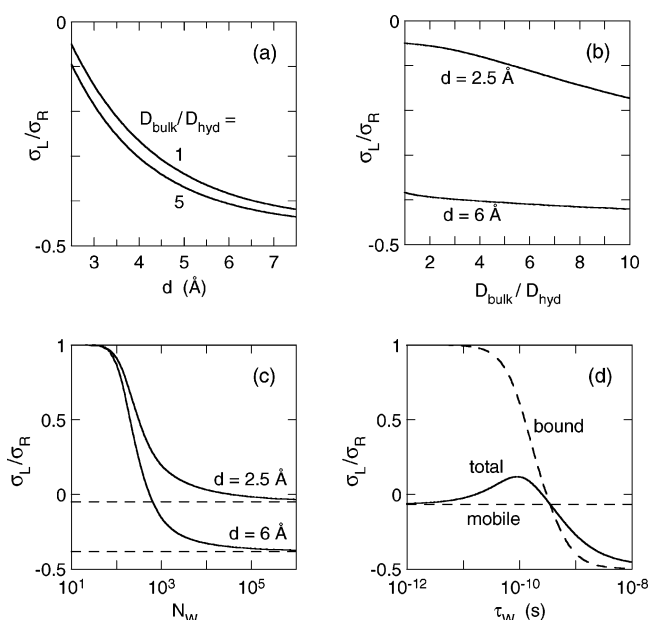


**Figure 3.** Ratio of water–oxytocin cross-relaxation rates in the laboratory ( $\sigma_L$ ) and rotating ( $\sigma_R$ ) frames at 600 MHz  $^1\text{H}$  NMR frequency predicted by the nonuniform diffusion model. Unless otherwise noted, the parameter values were taken from Table 2. The subfigures show the dependence of  $\sigma_L/\sigma_R$  on (a) the distance of closest approach between water and oxytocin protons, (b) the ratio of translational mobilities in hydration layer and bulk solvent, (c) the number of water molecules contributing to the cross-relaxation rates, and (d) the residence time of a single bound water molecule with the two water protons 3  $\text{\AA}$  from the oxytocin proton. In subfigure (c),  $D_{\text{hyd}} = D_{\text{bulk}}$  and the dashed lines represent the limit  $N_W \rightarrow \infty$ . In subfigure (d), the dashed curve and line give the  $\sigma_L/\sigma_R$  ratio produced by the single bound water molecule and all mobile water molecules, respectively.

BPTI identifies four internal water molecules buried in two small cavities.<sup>30</sup> These internal water molecules interact strongly with the protein and must contribute importantly to its stability. They should therefore be present also in solution. NOE studies have confirmed this expectation.<sup>8</sup> MRD studies have also determined the residence time ( $170 \pm 20\ \mu\text{s}$  at  $27\text{ }^{\circ}\text{C}$ ) and activation parameters for the singly buried water molecule (known as W122)<sup>5</sup> and provided bounds for the residence time ( $10\ \text{ns} \ll \tau_W < 1\ \mu\text{s}$  at  $27\text{ }^{\circ}\text{C}$ ) for at least two of the remaining three internal water molecules (known as W111–W113).<sup>41</sup>

The dynamics of water molecules interacting with the surface of BPTI (and other proteins) have not been characterized as thoroughly as the internal water molecules. MRD studies only yield a global measure of surface hydration in the form of the quantity  $N_\alpha \langle \tau_\alpha / \tau_{\text{bulk}} - 1 \rangle$ , where  $N_\alpha = 268$  is the number of water molecules in contact with the BPTI surface and  $\langle \tau_\alpha \rangle$  is the mean rotational correlation time for these water molecules. Previous  $^{17}\text{O}$  MRD studies yield  $N_\alpha \langle \tau_\alpha / \tau_{\text{bulk}} - 1 \rangle = 1200 \pm 100$  for BPTI at pH\* 5.2 and  $27\text{ }^{\circ}\text{C}$ ,<sup>42</sup> which translates into  $\langle \tau_\alpha \rangle / \tau_{\text{bulk}} = 5.5 \pm 0.4$ . The  $\tau_\alpha$  distribution is thought to have a weak long- $\tau_\alpha$  tail, so that the average  $\langle \tau_\alpha \rangle$  is strongly influenced by a relatively small number of more strongly perturbed water molecules, presumably located in surface pockets.<sup>6,7</sup> Yet even these strongly motionally retarded water molecules must have  $\tau_\alpha < 1\ \text{ns}$  (at  $27\text{ }^{\circ}\text{C}$ ), otherwise they would have been resolved in the MRD profile. Our strategy here is to study BPTI at low temperatures where  $\tau_\alpha$  for these strongly perturbed water

(41) Denisov, V. P.; Halle, B.; Peters, J.; Hörlein, H. D. *Biochemistry* **1995**, *34*, 9046–9051.

(42) Denisov, V. P.; Halle, B. *J. Mol. Biol.* **1995**, *245*, 682–697.



molecules exceeds 1 ns so that they can be observed directly in the MRD profile. In other words, by lowering the temperature, we gradually bring more water molecules into the MRD-accessible frequency window so that their correlation times ( $\tau_\beta$ ) can be determined, while the remaining, less perturbed, water molecules contribute to the decreasing average  $\langle\tau_\alpha\rangle$ .

NOE studies of protein surface hydration are scarce, and most of the published results refer to BPTI. To establish whether these NOE data are consistent with the new MRD data, we reanalyzed the most extensive set of NOE data, pertaining to surface hydration of BPTI at 4 °C,<sup>11,12,16,17</sup> with the aid of the nonuniform diffusion model.

**5.1. MRD Results.** We measured the longitudinal relaxation rate  $R_1$  of the water  $^2\text{H}$  and  $^{17}\text{O}$  magnetizations as a function of the resonance frequency  $\nu_0$  in an 8.3 mM BPTI solution at pH\* 5.2, dispersed in emulsion droplets to allow measurements in the deeply supercooled regime. The  $^2\text{H}$  and  $^{17}\text{O}$  MRD profiles at  $-10$  °C are shown in Figure 4a and b. At  $-30$  °C, where the fast  $^{17}\text{O}$  relaxation makes it difficult to obtain accurate measurements, we only report the  $^2\text{H}$  profile (Figure 4c). The parameter values resulting from the mono-Lorentzian fits (shown in the figures) are collected in Table 5. At these low temperatures (and pH\* 5.2), the labile BPTI protons exchange too slowly to contribute to the observed  $^2\text{H}$  magnetization.<sup>43</sup> Both the  $^2\text{H}$  and the  $^{17}\text{O}$  data therefore monitor water dynamics exclusively.

The  $^2\text{H}$  MRD data at  $-10$  °C (Figure 4a) are not well described by a mono-Lorentzian spectral density function (eq 3). For the estimated 0.5% standard deviation in  $R_1$ , the  $F$ -test<sup>26</sup> accepts a second Lorentzian component (labeled  $\gamma$ ) with a probability of 0.93. A bi-Lorentzian fit yields a low-frequency component with  $\tau_{\beta,\text{app}} = 11$  ns and  $(N_\beta S_\beta^2)_{\text{app}} = 1.5$ , a high-frequency component with  $\tau_\gamma = 1$  ns and  $N_\gamma S_\gamma^2 = 4$ , and a frequency-independent component with  $N_\alpha(\langle\tau_\alpha\rangle/\tau_{\text{bulk}} - 1) = 190$ . However, because only the  $R_1$  value at the highest frequency is strongly affected by the high-frequency  $\gamma$  dispersion, the parameters  $N_\gamma S_\gamma^2$  and  $N_\alpha(\langle\tau_\alpha\rangle/\tau_{\text{bulk}} - 1)$  exhibit a large covariance and cannot be determined individually with useful accuracy. To obtain a more accurate measure of surface hydration dynamics, we therefore performed a mono-Lorentzian fit to all data points except the one at highest frequency. The resulting parameter values are given in Table 5. As expected, the renormalized value of  $N_\alpha(\langle\tau_\alpha\rangle/\tau_{\text{bulk}} - 1)$  in Table 5, which now includes the  $\gamma$  component, is numerically close to the sum of the  $\alpha$  and zero-frequency  $\gamma$  components from the bi-Lorentzian fit.

The apparent correlation time,  $\tau_{\beta,\text{app}} = 10.7$  ns, of the low-frequency  $\beta$  component is close to the expected rotational correlation time,  $\tau_R = 14$  ns, of BPTI at this temperature (Table 1) and can be attributed to internal water molecules. A mono-Lorentzian fit to the  $^{17}\text{O}$  MRD data at  $-10$  °C (Figure 4b), again excluding the highest-frequency data point, yields parameter values close to the corresponding  $^2\text{H}$  values (Table 5). The small but significant differences can be explained by the higher  $^{17}\text{O}$  quadrupole frequency, making the fast-exchange condition more restrictive than for  $^2\text{H}$  (see the Supporting Information).

Turning now to the  $^2\text{H}$  dispersion at  $-30$  °C, we note that the mono-Lorentzian fit (with the highest-frequency point excluded) yields a  $(N_\beta S_\beta^2)_{\text{app}}$  value twice as large as at  $-10$  °C,

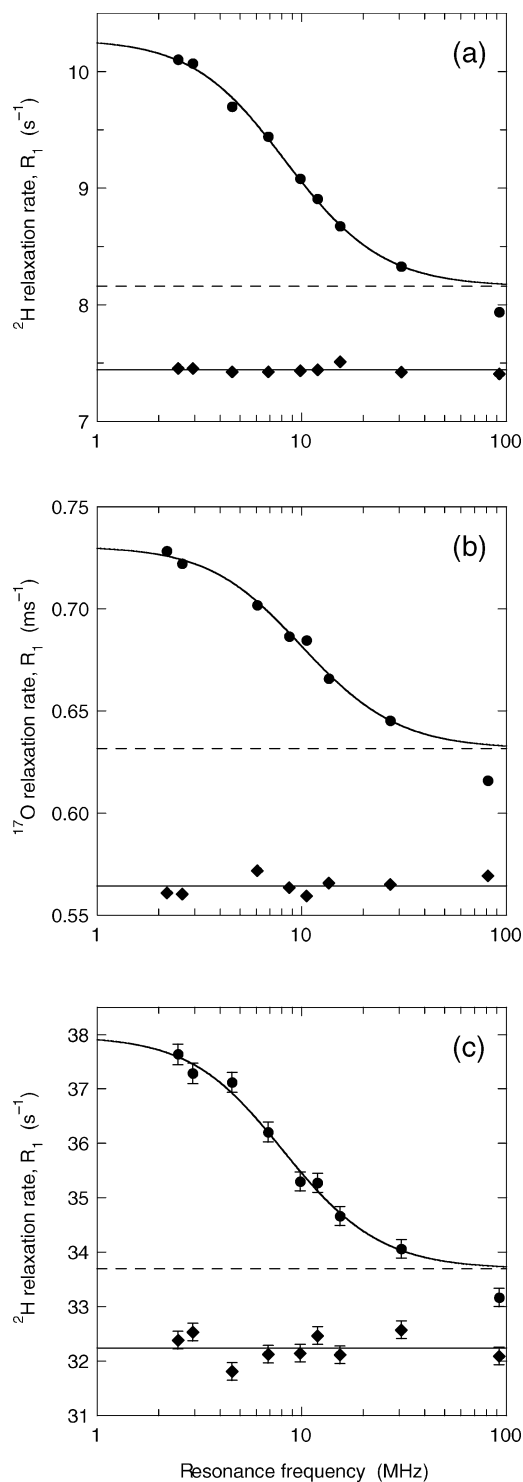


**Figure 4.** Water  $^2\text{H}$  and  $^{17}\text{O}$  MRD profiles from an emulsified aqueous solution of 8.3 mM BPTI at pH\* 5.2: (a)  $^2\text{H}$  profile at  $-10$  °C; (b)  $^{17}\text{O}$  profile at  $-10$  °C; and (c)  $^2\text{H}$  profile at  $-30$  °C. The dispersion curves resulted from fits according to eqs 2 and 3, with the highest-frequency data point excluded. In (a) and (b), the uncertainty in  $R_1$  is comparable to the size of the data symbols. The solid line represents the mean of the measured  $R_{\text{bulk}}$  values, and the dashed line corresponds to  $R_{\text{bulk}} + \alpha$ .

whereas  $\tau_{\beta,\text{app}}$  is virtually the same (Figure 4c and Table 5). This means that the dispersion is dominated by water molecules at the protein surface, rather than by internal water molecules. Indeed, on the basis of residence times and activation energies established at higher temperatures, we do not expect any of the four internal water molecules to contribute significantly at  $-30$

(43) Denisov, V. P.; Halle, B. *J. Mol. Biol.* **1995**, *245*, 698–709.

**Table 5.** MRD Results for BPTI at  $-10$  and  $-30$  °C

$T$ (°C)	nucleus	$R_{\text{bulk}}^a$ ( $\text{s}^{-1}$ )	$(N_{\beta}S_{\beta}^2)_{\text{app}}^b$	$\tau_{\beta,\text{app}}^b$ (ns)	$N_{\alpha}(\langle\tau_{\alpha}\rangle/\tau_{\text{bulk}} - 1)$	$\langle\tau_{\alpha}\rangle/\tau_{\text{bulk}}^c$
$-10$	$^2\text{H}$	7.44	$1.7 \pm 0.1$	$10.7 \pm 0.7$	$620 \pm 50$	$3.3 \pm 0.2$
$-10$	$^{17}\text{O}$	564	$1.2 \pm 0.2$	$8.9 \pm 0.9$	$760 \pm 60$	$3.8 \pm 0.2$
$-30$	$^2\text{H}$	32.2	$3.3 \pm 0.4$	$11 \pm 1$	$290 \pm 40$	$2.1 \pm 0.2$

<sup>a</sup> Mean of  $R_{\text{bulk}}$  at all frequencies, 0.5% standard deviation. <sup>b</sup> Apparent quantities defined by eq S1 in the Supporting Information. <sup>c</sup> Calculated from eq 4 with  $N_{\alpha} = 268$ .

°C (see the Supporting Information). We therefore attribute the  $^2\text{H}$  dispersion at  $-30$  °C entirely to water molecules interacting with the external surface of BPTI. Because  $\tau_{\beta} = 11$  ns is much shorter than the rotational correlation time of BPTI at  $-30$  °C (Table 1), these water molecules must have residence times in the range 10–15 ns (see eq 6).

The value  $N_{\beta}S_{\beta}^2 = 3.3 \pm 0.4$  implicates three such water molecules, or more if they are orientationally disordered. These must be the water molecules responsible for the  $\gamma$  dispersion at  $-10$  °C (with  $\tau_{\text{w}} \approx 1$  ns). Indeed, bi-Lorentzian fits to the  $^2\text{H}$  and  $^{17}\text{O}$  data at  $-10$  °C yield  $N_{\gamma}S_{\gamma}^2 = 3-4$  (albeit with large errors). A  $\gamma$  dispersion is also evident at  $-30$  °C (Figure 4c), indicating that a new group of water molecules acquire residence times of about 1 ns at this temperature. In the mono-Lorentzian fit, these water molecules are included in the frequency-independent parameter  $N_{\alpha}(\langle\tau_{\alpha}\rangle/\tau_{\text{bulk}} - 1)$ , which corresponds to a rotational retardation factor  $\langle\tau_{\alpha}\rangle/\tau_{\text{bulk}} = 2.1 \pm 0.2$ . For the vast majority of the  $N_{\alpha} = 268$  water molecules in the hydration layer,  $\langle\tau_{\alpha}\rangle/\tau_{\text{bulk}}$  must therefore be less than 2.1. With  $\tau_{\text{bulk}} = 4$  ps at 4 °C (the temperature of the NOE experiments on BPTI, see below),<sup>39</sup> the MRD-derived retardation factor of 2 corresponds to an average residence time of only  $2 \times 3 \times 4 = 24$  ps (where the factor 3 converts to the rank-1 correlation time).

**5.2. NOE Results.** To determine whether the MRD and NOE methods yield mutually consistent results for the surface hydration of BPTI, we present here a reanalysis in terms of the nonuniform diffusion model of an extensive set of NOE data, acquired at 4 °C on a 20 mM BPTI solution (with 10%  $\text{D}_2\text{O}$ ) at pH\* 3.5.<sup>11,12,16,17</sup> These data were recorded with homonuclear 3D NOESY-TOCSY and ROESY-TOCSY experiments at a  $^1\text{H}$  resonance frequency of 500 MHz.<sup>16</sup> Table 5 of ref 17 lists 44 BPTI-water cross-peaks with positive  $\sigma_{\text{L}}$  values. For one-half of these cross-peaks, the (inconsistent) uniform diffusion model<sup>32</sup> suggests residence times in the range 100–500 ps based on the experimental  $\sigma_{\text{L}}/\sigma_{\text{R}}$  ratios.<sup>17</sup> In contrast, the nonuniform diffusion model predicts much shorter residence times, in agreement with the MRD data.

As intramolecular NOEs to labile protons yield negative  $\sigma_{\text{L}}$  rates, water–protein cross-peaks with positive  $\sigma_{\text{L}}$  values cannot be attributed exclusively to exchange-relayed NOEs, that is, NOEs with labile protein protons appearing at the water chemical shift due to rapid exchange. Cross-peaks with positive  $\sigma_{\text{L}}$  rates thus present unambiguous evidence for NOEs with water.<sup>4</sup> As positive  $\sigma_{\text{L}}$  rates are invariably small, the size of the corresponding cross-peaks is easily affected by competing magnetization transfer pathways, in particular exchange-relayed NOEs. Calculations with the nonuniform diffusion model indicate that a labile proton at a distance of about 5 Å can affect both  $\sigma_{\text{L}}$  and  $\sigma_{\text{R}}$  rates significantly. An analysis of the crystal structure 5PTI<sup>30</sup> shows that for 21 of the 44 reported cross-

peaks,<sup>17</sup> at least one proton is within 5 Å of a hydroxyl proton (10), a carboxyl oxygen (10), or a proton in one of the three long-lived internal water molecules (2). For three more cross-peaks, there are hydroxyl, carboxyl, and/or internal water protons within 5–6 Å. In a conservative approach, these cross-peaks were excluded from the following analysis of surface hydration, although NOEs to carboxyl protons are usually elusive.<sup>44</sup>

For the remaining 20 cross-peaks, calculations based on the nonuniform diffusion model yield  $\sigma_{\text{R}} = 0.06 \pm 0.01 \text{ s}^{-1}$  and a water contribution to  $\sigma_{\text{R}}$  between 64% and 99%. The parameter values used in the calculations are given in Table 2 and rationalized in the Supporting Information. As all of the examined BPTI protons are highly exposed, we used  $d = d_{\text{min}} = 2.5$  Å for all of them. This is in contrast to oxytocin, where variations in  $d$  (or solvent exposure) were found to be the major cause of variation in  $\sigma_{\text{L}}/\sigma_{\text{R}}$  (section 3.2). For BPTI, variations in the calculated  $\sigma_{\text{L}}/\sigma_{\text{R}}$  ratio are thus entirely due to contributions to the cross-relaxation rates from dipole–dipole couplings with labile BPTI protons and internal water protons (see above), both of which exchange with bulk water during the mixing time. As for oxytocin, we make the identification  $D_{\text{bulk}}/D_{\text{hyd}} = \langle\tau_{\alpha}\rangle/\tau_{\text{bulk}}$ , but with  $D_{\text{bulk}}/D_{\text{hyd}} = 2$  (Table 5) and  $\delta = 2.4$  Å (corresponding to a sphere of radius 15 Å covered by  $N_{\alpha} = 268$  hydration water molecules). The experimental and calculated  $\sigma_{\text{L}}/\sigma_{\text{R}}$  ratios for the 20 cross-peaks with dominant (>60%) calculated water contributions to  $\sigma_{\text{R}}$  are given in Table S1 in the Supporting Information. In agreement with the experimental  $\sigma_{\text{L}}/\sigma_{\text{R}}$  ratios, the calculated values are positive, although on average a factor of 2 smaller. The overall correlation between experimental and calculated  $\sigma_{\text{L}}/\sigma_{\text{R}}$  values is, however, weak ( $r = 0.4-0.5$ ). The most plausible explanation is that too small  $\sigma_{\text{R}}$  values were measured from the ROE-TOCSY spectra, which had been recorded without off-resonance compensation pulses<sup>45,46</sup> and with ROE mixing times of 25 ms, where the onset of transverse relaxation may no longer have been negligible. This explanation is further supported by  $\sigma_{\text{L}}/\sigma_{\text{R}}$  values of 1.0, as reported for 10 of the 44 cross-peaks.<sup>17</sup> In the diffusion model,  $\sigma_{\text{L}}/\sigma_{\text{R}} = 1.0$  is only obtained in the unphysical limit  $d \rightarrow 0$ , where the contribution from long-range dipolar couplings with bulk water becomes negligible (see Figure S3c). The calculations in Figure S3 indicate that  $\sigma_{\text{L}}/\sigma_{\text{R}}$  should not be much larger than 0.5 under the conditions of the NOE study. This is a consequence of long-range dipole–dipole couplings to bulk water, which are even more important for BPTI than for oxytocin. (This can be seen by comparing Figures 3c and S3c, where, for any  $N_{\text{W}}$ ,  $\sigma_{\text{L}}/\sigma_{\text{R}}$  is further from its  $N_{\text{W}} \rightarrow \infty$  limit for BPTI than for oxytocin.) The slower convergence of  $\sigma_{\text{L}}/\sigma_{\text{R}}$  with  $N_{\text{W}}$  for BPTI is mainly due to the 5-fold higher bulk water mobility at the higher temperature of the BPTI study (Table 2). The larger influence of long-range dipolar couplings makes  $\sigma_{\text{L}}/\sigma_{\text{R}}$  less sensitive to hydration dynamics for BPTI than for oxytocin (Figures 3b and S3b).

## 6. Concluding Discussion

**6.1. Proteins versus Small Molecules.** For many years, the hydration layer surrounding proteins was thought to be much

(44) Liepinsh, E.; Rink, H.; Otting, G.; Wüthrich, K. *J. Biomol. NMR* **1993**, *3*, 253–257.

(45) Griesinger, C.; Ernst, R. R. *J. Magn. Reson.* **1987**, *75*, 261–271.

(46) Otting, G.; Liepinsh, E.; Farmer, B. T.; Wüthrich, K. *J. Biomol. NMR* **1991**, *1*, 209–215.

**Table 6.** Rotational Retardation of Hydration Water from  $^2\text{H}$  and  $^{17}\text{O}$  Relaxation

solute	$N_{\text{hyd}}^a$	$\langle\tau_{\text{hyd}}\rangle/\tau_{\text{bulk}}$	$T(^{\circ}\text{C})$	ref
BPTI <sup>b</sup>	265	$3.3 \pm 0.2$	-10	this work
BPTI <sup>b</sup>	265	$2.1 \pm 0.2$	-30	this work
oxytocin	73	$3.3 \pm 0.2$	-25	this work
glycine	12.4	$1.3^c$	25	53
alanine	14.4	$1.7^c$	25	53
valine	17.7	$2.1^c$	25	53
leucine	19.5	$2.4^c$	25	53
methanol	12	$1.4^d$	25	54
<i>n</i> -propanol	17	$1.8^d$	25	54
<i>t</i> -butanol	19	2.2	25	54
benzene	23	1.6	25	55

<sup>a</sup> Number of water molecules in contact with solute, estimated as solvent-accessible area ( $1.4 \text{ \AA}$  probe) divided by  $15 \text{ \AA}^2$ . <sup>b</sup> External surface, including ( $-10^{\circ}\text{C}$ ) or excluding ( $-30^{\circ}\text{C}$ ) about 3 water molecules in surface pockets. <sup>c</sup> Obtained from original  $^{17}\text{O}$  relaxation data using the  $N_{\text{hyd}}$  values given here (based on solvent-accessible areas). <sup>d</sup> These results agree quantitatively with results derived from  $^{17}\text{O}$ -induced dipolar  $^1\text{H}$  relaxation,<sup>56</sup> demonstrating that any perturbation of the water  $^{17}\text{O}$  quadrupole coupling constant by the solute is unimportant.

less mobile than bulk water.<sup>47</sup> Such a view implies that a protein surface has a much larger effect on water dynamics than a small solute. While recent NMR studies<sup>7</sup> and computer simulations<sup>35,48–50</sup> have demonstrated that water in the hydration layer is only weakly perturbed by the protein, few experimental studies have directly compared the hydration of proteins and smaller solutes.  $^2\text{H}$  and  $^{17}\text{O}$  MRD studies invariably yield a rotational retardation factor  $\langle\tau_{\text{hyd}}\rangle/\tau_{\text{bulk}}$  in the range 4–6 for the hydration layer of globular proteins at  $27^{\circ}\text{C}$ .<sup>6,7</sup> This is only a factor of 2–3 more than for amino acids or other molecules of similar size (Table 6). It has been suggested that the larger value for proteins, which is an average over hundreds of water molecules, is dominated by a small number of strongly motionally retarded water molecules located in pockets and clefts on the protein surface.<sup>6,7</sup> The important role of surface topography in controlling hydration structure<sup>51,52</sup> and dynamics<sup>48–50</sup> has also emerged from molecular simulations. The low-temperature MRD data presented here provide direct experimental support for this view.

As the temperature is lowered sufficiently for a group of strongly motionally retarded water molecules to enter the accessible MRD frequency window (correlation time  $> 1$  ns), the remaining water molecules at the protein surface which are then responsible for the high-frequency excess relaxation rate are less perturbed on average. Between  $-10$  and  $-30^{\circ}\text{C}$ , about three strongly perturbed water molecules thus move into the MRD window, and, as a consequence,  $\langle\tau_{\text{hyd}}\rangle/\tau_{\text{bulk}}$  decreases from 3.3 to 2.1 (Table 5). Also at  $-30^{\circ}\text{C}$ , the MRD data indicate that a few water molecules have correlation times around 1 ns (Figure 4c). If there are three such water molecules,  $\langle\tau_{\text{hyd}}\rangle/\tau_{\text{bulk}}$  would be further reduced to 1.8 for the remaining ca. 260 water molecules in the hydration layer. Neither of these values (2.1 or 1.8) differs significantly from the values found for apolar amino acids or short-chain alcohols (Table 6). With a few special hydration sites in deep surface pockets and clefts excluded, a

protein surface thus appears, on average, to have the same effect on water dynamics as a typical small solute: a two-fold retardation.

This conclusion is based on a comparison of BPTI hydration at  $-30^{\circ}\text{C}$  with small-molecule hydration at  $25^{\circ}\text{C}$ . If the activation energies of  $\tau_{\text{hyd}}$  and  $\tau_{\text{bulk}}$  differ significantly, this comparison may not be valid. For the alcohols, temperature-dependent  $^{17}\text{O}$  relaxation data have been reported for the range  $1–50^{\circ}\text{C}$ ,<sup>54</sup> and for benzene  $^2\text{H}$  data are available from  $-18$  to  $30^{\circ}\text{C}$ .<sup>55</sup> These data show that, for nonpolar solutes,  $\tau_{\text{hyd}}$  has a significantly stronger temperature dependence than  $\tau_{\text{bulk}}$ . Extrapolating the data to  $-30^{\circ}\text{C}$ , we find  $\langle\tau_{\text{hyd}}\rangle/\tau_{\text{bulk}}$  values of 3.5, 9, 14, and 6 for methanol, propanol, *tert*-butyl alcohol, and benzene, respectively. The usual explanation of this phenomenon is that a clathrate-like hydration shell forms around such nonpolar solutes, with water–water hydrogen bonds that are stronger than in bulk water and considerably more long-lived because of the inability of the apolar (part of the) solute to participate in the fluctuating hydrogen-bond network.

In contrast to these small solutes, our low-temperature MRD results for BPTI show that  $\langle\tau_{\text{hyd}}\rangle/\tau_{\text{bulk}}$  decreases at lower temperatures. We have rationalized this decrease in terms of a few strongly perturbed water molecules that give rise to an observable dispersion at low temperatures. The remaining high-frequency excess relaxation rate is not compatible with a strong temperature dependence of the kind seen for small nonpolar solutes. We conclude, therefore, that clathrate-like hydration structures are not prevalent at the surface of BPTI. This is understandable, because few side chains protrude from the surface to the extent that they can be surrounded by a clathrate cage in the same way as for a small solute. For BPTI, and for most other native globular proteins,<sup>57,58</sup> about 60% of the solvent-accessible surface area is contributed by nonpolar atoms. The inferred absence of classical hydrophobic hydration structures at the surface of BPTI, which would have caused  $\langle\tau_{\text{hyd}}\rangle/\tau_{\text{bulk}}$  to increase strongly at lower temperatures, suggests that the entropic penalty for the residual exposure of nonpolar groups at the surface of the native protein may be smaller than expected on the basis of small-molecule solvation thermodynamics (for the same overall nonpolar surface area). If this is true, hydrophobic side chains stabilize native protein structures not only through burial in the protein core, but also, albeit to a lesser extent, when partly exposed at the protein surface.

For oxytocin, we find  $\langle\tau_{\text{hyd}}\rangle/\tau_{\text{bulk}} = 3.3$  at  $-25^{\circ}\text{C}$ , as compared to 2.1 for BPTI at  $-30^{\circ}\text{C}$ . This difference suggests that oxytocin contains one or a few more strongly motionally retarded hydration water molecules that make a substantial contribution to  $\langle\tau_{\text{hyd}}\rangle/\tau_{\text{bulk}}$ . Indeed, measurements at 92 MHz ( $^2\text{H}$ ) and 81 MHz ( $^{17}\text{O}$ ) are significantly below the average level shown in Figures 1 and 2. As in the case of BPTI, this indicates one or two water molecules with a correlation time of about 1 ns at  $-25^{\circ}\text{C}$ . If these are excluded,  $\langle\tau_{\text{hyd}}\rangle/\tau_{\text{bulk}}$  would decrease to about 2, as for BPTI.

- (47) Kuntz, I. D.; Kauzmann, W. *Adv. Protein Chem.* **1974**, *28*, 239–345.  
 (48) Makarov, V. A.; Andrews, B. K.; Smith, P. E.; Pettitt, B. M. *Biophys. J.* **2000**, *79*, 2966–2974.  
 (49) Luise, A.; Falconi, M.; Desideri, A. *Proteins* **2000**, *39*, 56–67.  
 (50) Sterpone, F.; Ceccarelli, M.; Marchi, M. *J. Mol. Biol.* **2001**, *311*, 409–419.  
 (51) Cheng, Y.-K.; Rossky, P. J. *Nature* **1998**, *392*, 696–699.  
 (52) Carey, C.; Cheng, Y.-K.; Rossky, P. J. *Chem. Phys.* **2000**, *258*, 415–425.

- (53) Ishimura, M.; Uedaira, H. *Bull. Chem. Soc. Jpn.* **1990**, *63*, 1–5.  
 (54) Ishihara, Y.; Okouchi, S.; Uedaira, H. *J. Chem. Soc., Faraday Trans.* **1997**, *93*, 3337–3342.  
 (55) Nakahara, M.; Yoshimoto, Y. *J. Phys. Chem.* **1995**, *99*, 10698–10700.  
 (56) Ludwig, R. *Chem. Phys.* **1995**, *195*, 329–337.  
 (57) Harpaz, Y.; Gerstein, M.; Chothia, C. *Structure* **1994**, *2*, 641–649.  
 (58) Murphy, L. R.; Matubayasi, N.; Payne, V. A.; Levy, R. M. *Fold. Des.* **1998**, *3*, 105–118.

In summary, our analysis of the new MRD data indicates that more than 95% of the water molecules in contact with the surfaces of BPTI or oxytocin have rotational correlation times that are merely a factor 2 longer than in bulk water at the low temperatures investigated here. Because of the difficulty of forming complete clathrate cages at protein or peptide surfaces, it appears that  $\langle\tau_{\text{hyd}}\rangle/\tau_{\text{bulk}}$  has a much weaker temperature dependence than for small apolar molecules. In any case, the rotational retardation should not be larger than a factor of 2 at room temperature. Because rotation and translation of water are both governed by hydrogen-bond dynamics, these motions should be retarded to the same extent. Consequently, the mean residence time is only increased by a factor of 2 for more than 95% of the water molecules at the surface of BPTI or oxytocin, in essential agreement with the results of molecular simulation studies of protein hydration dynamics at room temperature.<sup>48–50</sup>

**6.2. Interpretation of Intermolecular NOEs.** As argued here and elsewhere,<sup>15</sup> intermolecular NOEs between water and solute protons are affected by long-range dipole–dipole couplings with a large number of water molecules outside the hydration layer. Even though individual dipole couplings with remote water molecules are much weaker than couplings with nearby water molecules, they are more numerous and are modulated more slowly at a rate that depends on the internuclear separation and the diffusion coefficient as  $D_T/r^2$ . Quantitative information about hydration water mobility can be extracted from intermolecular NOEs only with the aid of a model that explicitly incorporates dynamic heterogeneity, for example, by assigning different values to the diffusion coefficient of hydration water and bulk water. In the present work, we have used such a nonuniform diffusion model to interpret intermolecular NOE data on surface hydration dynamics for oxytocin and BPTI. Moreover, we have compared the results of this analysis to MRD results obtained on the same systems.

Our model calculations show that the sign reversal observed for water–oxytocin NOEs at subzero temperatures<sup>18</sup> can be explained by the reduced diffusion coefficient of bulk water. A negative NOE should therefore not be taken as evidence for substantially prolonged residence times of hydration water. Individual hydration water molecules can dominate the NOE only if they are located near the observed solute proton and if their mobility is very much reduced as compared to bulk water. This is the case for water molecules trapped in cavities inside proteins, like the four internal water molecules in BPTI,<sup>8</sup> and for water molecules in the narrowed minor groove of AT-tracts in *B*-DNA.<sup>19,59,60</sup> In such cases, water–biomolecule NOEs can be interpreted in terms of an intramolecular spectral density function (eqs 6 and 8), where the strong distance dependence ( $r_{\text{HH}}^{-6}$ ) provides a geometric constraint on the location of long-lived water molecules.

The MRD results presented here show that the vast majority of water molecules in contact with the surface of BPTI, and presumably all proteins, have a mobility that is only marginally (on average, a factor of 2) lower than in bulk water. According to our model calculations, such small dynamic hydration effects cannot be quantified by intermolecular NOEs with surface protons. The calculations indicate that the observed variation

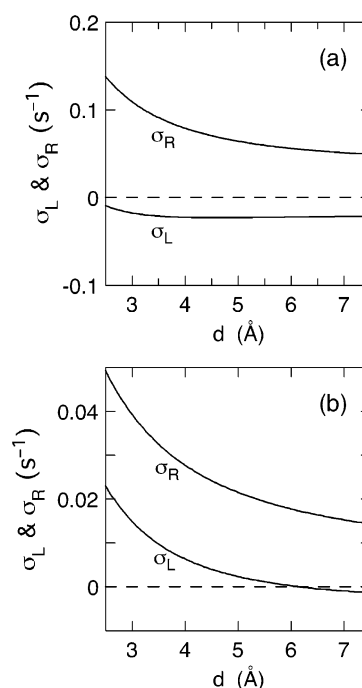


**Figure 5.** Variation of the intermolecular cross-relaxation rates in the laboratory ( $\sigma_L$ ) and rotating ( $\sigma_R$ ) frames with the distance of closest approach for (a) oxytocin at  $-25\text{ }^\circ\text{C}$  and (b) BPTI at  $4\text{ }^\circ\text{C}$ , as predicted by the nonuniform diffusion model with parameter values from Table 2. In comparison, the intramolecular cross-relaxation rates of a proton pair with separation  $3.0\text{ }\text{\AA}$  would be  $\sigma_L = -1.04\text{ s}^{-1}$  and  $\sigma_R = 2.08\text{ s}^{-1}$  in the case of oxytocin and  $-0.52$  and  $1.04\text{ s}^{-1}$ , respectively, in the case of BPTI.

of the ratio  $\sigma_L/\sigma_R$  of cross-relaxation rates for the surface protons of BPTI is mainly due to variations in the burial depth or solvent-accessibility of the observed BPTI proton, rather than to variations in the mobility of hydration water. This conclusion is in line with a previous theoretical study.<sup>33</sup> Nonetheless, the observation of positive NOEs with the surface protons of BPTI (at temperatures above  $0\text{ }^\circ\text{C}$ ) provides an upper bound of ca. 1 ns for the residence time of water molecules within  $3\text{--}4\text{ }\text{\AA}$  of these protons (see Figure S3d), as concluded previously.<sup>11</sup>

If intermolecular protein–water NOEs are dominated by long-range dipole couplings to bulk water molecules, then NOEs with internal protons should not be much weaker than for surface protons. This expectation is confirmed by the oxytocin results (Table 4), where  $\sigma_R$  is only a factor 2–3 smaller for the core protons ( $d = 5\text{--}8\text{ }\text{\AA}$ ) than for the peripheral protons ( $d = 2.5\text{ }\text{\AA}$ ). As seen from Figure 5a, the laboratory-frame cross-relaxation rate  $\sigma_L$  is nearly independent of  $d$  in the range  $3\text{--}8\text{ }\text{\AA}$ . The difference in the ratio  $\sigma_L/\sigma_R$  between the two classes of protons is therefore mainly due to the variation in  $\sigma_R$ . A similar picture would hold for BPTI at  $-25\text{ }^\circ\text{C}$ . However, at the higher temperature ( $4\text{ }^\circ\text{C}$ ) of the NOE experiments on BPTI,<sup>11,16</sup> no cross-peaks between water and internal protons were observed that could not be attributed to nearby internal water molecules or labile protons. The absence of long-range water contributions to NOESY cross-peaks can be explained by the 5-fold faster bulk water diffusion (as compared to the oxytocin experiments at  $-25\text{ }^\circ\text{C}$ ), rendering  $\sigma_L$  more sensitive to the distance of closest approach and placing the zero-crossing at  $d \approx 6\text{ }\text{\AA}$  (Figure 5b). The absence of long-range water contributions to ROESY cross-peaks, on the other hand, can be attributed to fast transverse relaxation and spin diffusion, suppressing the NOE build-up

(59) Liepinsh, E.; Otting, G.; Wüthrich, K. *Nucleic Acids Res.* **1992**, *20*, 6549–6553.

(60) Halle, B.; Denisov, V. P. *Biopolymers* **1998**, *48*, 210–233.

during the mixing time.<sup>31,61</sup> Even if the consequent sensitivity loss could be alleviated, for example, by using an isotope labeled protein, the small magnitude of the direct water contribution to  $\sigma_R$  for internal protons (Figure 5) would make the direct long-range NOE susceptible to competition from exchange-relayed NOEs with labile protein protons and internal water protons at separations of up to 6–7 Å. In BPTI, only about 10 deeply buried ( $d > 5$  Å) protons are thus predicted to have a dominant contribution to  $\sigma_R$  from direct water NOEs.

(61) Brown, L. R.; Farmer, B. T. *Methods Enzymol.* **1989**, *176*, 199–216.

**Acknowledgment.** This work was supported by the Swedish Research Council. G.O. acknowledges a Federation Fellowship from the Australian Research Council.

**Supporting Information Available:** Experimental protocol for NOE experiments on oxytocin, estimates of parameter values used for NOE calculations, further details about the analysis of low-temperature MRD data on BPTI, and a more complete account of NOE calculations for BPTI (PDF). This material is available free of charge via the Internet at <http://pubs.acs.org>.

JA038325D